Measurement Science and Technology

TOPICAL REVIEW

High dynamic range 3D measurements with fringe projection profilometry: a review

Meas. Sci. Technol. 29 (2018) 122001 (19pp) https://doi.org/10.1088/1361-6501/aae4fb

Topical Review

High dynamic range 3D measurements with fringe projection profilometry: a review

Shijie Feng[1,2], Liang Zhang[1,2], Chao Zuo[1,2], Tianyang Tao[1,2], Qian Chen[1] and Guohua Gu[1]

[1] Jiangsu Key Laboratory of Spectral Imaging & Intelligent Sense, Nanjing University of Science and Technology, Nanjing, Jiangsu Province 210094, People's Republic of China
[2] Smart Computational Imaging (SCI) Laboratory, Nanjing University of Science and Technology, Nanjing, Jiangsu Province 210094, People's Republic of China

E-mail: ShijieFeng@njust.edu.cn, zuochao@njust.edu.cn and chenqian@njust.edu.cn

Received 24 March 2018, revised 12 September 2018
Accepted for publication 28 September 2018
Published 6 November 2018

Abstract

In optical metrology, fringe projection is considered to be one of the most reliable techniques for recovering the shape of objects. For this technique, however, it is challenging to measure objects with a large variation in surface reflectivity, e.g. a scenario containing both dark and bright objects. Researchers have thus developed various approaches to high dynamic range (HDR) three-dimensional (3D) measurements over the years. In this paper, we present an overview of these techniques, as well as a new and definitive classification for them. We implement a set of representative techniques to measure objects with different characteristics of reflectance and discuss the advantages and constraints of the techniques according to the comparative results. Moreover, challenging problems and future research directions are discussed to advance HDR 3D measurement techniques.

Keywords: high dynamic range, 3D measurements, fringe projection, image saturation, phase-shifting profilometry

(Some figures may appear in colour only in the online journal)

1. Introduction

Geometry information plays a significant role in various fields, including medical imaging, industrial manufacturing, homeland security, and entertainment. Three-dimensional (3D) shape measurements have received extensive attention over the past decades [1–5]. A coordinate measuring machine (CMM) is a typical device that can measure the 3D shape of physical objects by sensing the points on the surface of the object with a mechanical probe [6–8]. Although the system has the advantage of high accuracy, it is fragile for soft objects due to the nature of its physical contact. Also, it is restricted to a slow measuring speed, since it needs to perform point-by-point measurements.

In contrast, optical 3D shape measuring techniques that extract geometry information from received light signals, e.g. digital images, can sense the surface shape without physical contact [9–16]. Moreover, their measuring speed for entire measured objects can reach hundreds or even thousands of frames per second [17–20], which significantly improves the efficiency of the 3D acquisition. Therefore, optical techniques are more flexible and efficient than the traditional CMM technique. Among the optical techniques, fringe projection profilometry (FPP) has proven to be one of the most promising [21–28]. In practice, the simplest FPP system consists of a camera, a projector, and a computer. Controlled by the computer, a set of well-designed fringe patterns are projected onto measured objects. At the same time, the camera captures the

HDR 3D imaging by FPP	Equipment-based techniques (using highlight-free images)	Camera-based	Refs.[46-54]
		Projector-based	Refs.[55-65]
		Additional-equipment-based	Refs.[66-69]
		Hybrid techniques	Refs.[70-73]
	Algorithm-based techniques (using saturated images)	Specific algorithms	Refs.[74-81]

Figure 1. The proposed classification.

corresponding deformed fringe patterns, which contain the phase information of the projected fringes. The computer then performs decoding algorithms to extract the phase information from the captured images and maps it to real-world 3D coordinates of the object through triangulation [29–34].

As an image-based 3D shape measuring technique, FPP assumes measured surfaces exhibit a diffuse reflection and usually considers low-reflective (dark) areas and highlight spots (specular reflection) as outliers [35–39]. The reason is that the dark areas are often captured with low-contrast fringe patterns, and the reflective surfaces are usually captured as pure white pixels due to the intense reflected light. Thus, it is difficult to capture desired fringe patterns for both kinds of the surfaces. Consequently, it is hard to obtain reliable 3D reconstructions. However, in the real world, many objects are not ideally Lambertian and have low- and high-reflective surfaces simultaneously. The conventional assumption tends to restrict the application of FPP.

To solve the problem of saturation, intuitively, one can spray a thin layer of diffuse powder to cover specular highlights on the measured objects. However, not all objects are fit for spraying. The method is only preferred when the effect of the sprayed layer on the measuring accuracy can be ignored. To measure objects without changing their intrinsic appearances, researchers developed various approaches to high dynamic range (HDR) fringe projection techniques. As a straightforward method, gamma correction can be applied for extension of the dynamic range. Humans perceive light in a nonlinear manner (power-law response). Thus, for visual quality, digital devices, e.g. projectors, cameras, and displays, are often manufactured with gamma distortion in which the transform of light intensity can be expressed as $I_{\text{out}} = I_{\text{in}}^{\gamma}$. For example, typically a digital device has a gamma (γ) which usually equals 2.2. In this case, dark objects (with small I_{in}) will be measured with compressed and smaller output intensity, which restricts the dynamic range of measurement and makes it difficult to differentiate details on these surfaces. Hence, we need to correct the gamma distortion to increase the dynamic range of captured images. Traditionally, the photometric calibration technique [40] was used to quantify the nonlinearity of a measuring system. A target plane is illuminated by the projector with a full range of known luminance, and simultaneously the intensities are captured by the camera. A response curve of the overall system can then be plotted and employed to compensate for the effect of the nonlinearity. But, the whole calibration process is time consuming and laborious. To avoid the calibration, Farid [41] suggested a blind gamma correction technique by which the gamma distortion can be blindly estimated using tools based on polyspectral analysis. Also avoiding the need for calibration, Guo *et al* [42] proposed an iterative gamma correction method with the assist of statistical analysis of captured distorted fringe images. In addition, correction techniques based on look-up table mapping [43], phase error analysis [44], and gamma estimation from phase-shifting methods [45] were presented to efficiently and robustly remove the effect of gamma. Practically, for applications of fringe projection, gamma correction not only extends the dynamic range of captured patterns but also improves the accuracy of 3D reconstruction. Due to the nonlinearity caused by gamma, the sinusoidal pattern tends to be captured with a distorted shape, which introduces undesired artifacts into reconstruction results. Thus, the accuracy of measurements can also be improved once gamma is corrected.

Although gamma correction can enhance the dynamic range by removing the nonlinearity of the measuring system, it is hard for it to attack the problem fundamentally. Thus, more in-depth research was carried out to deal with the problem. In this paper, we present an overview of this research and classify the developed techniques into two groups: equipment-based techniques and algorithm-based techniques, as can be seen in figure 1. The two groups differ in the captured fringe images from which the geometry information is extracted. For the group of equipment-based techniques [46–73], the emphasis is to find the optimal parameters of the equipment used, e.g. the proper exposure time of the camera or the desired brightness of the projected light, for capturing ideal fringe images for both the low- and high-reflective surfaces. For the group of algorithm-based techniques [74–81], on the other hand, it is not necessary to capture ideal (e.g. specular-free) images. Without any adjustments to the hardware equipment, it merely relies on well-designed algorithms to extract the depth information from the raw fringe images. In the literature of FPP, we find that there are many more techniques based on adjustments to the equipment than ones only depending on a certain algorithm. Therefore, we further subdivide the techniques of the first group according to the specific equipment they adjust: camera-based techniques [46–54], projector-based techniques [55–65], additional equipment-based techniques [66–69], and hybrid techniques [70–73]. For camera-based techniques, HDR 3D imaging is achieved by changing the exposure time of the camera or by adjusting the viewpoint of the camera for capturing the desired fringe images. Techniques based on the adjustment of the projector rely on the fact that FPP is an active 3D measurement strategy, which allows ideal fringe images to be acquired through appropriate adjustments to the projected light intensity. In addition, the HDR 3D measurements can be carried out by introducing additional equipment into the FPP system as well, e.g. polarizers which can remove specularity. Lastly, some approaches are based on combinations of the mentioned strategies, e.g. not only adjusting the parameters of the system but also introducing additional equipment, which is useful for complex scenarios.

Considering the different merits and features of the mentioned techniques, we believe a thorough understanding of them will be of great importance to the selection of a proper HDR 3D measurement technique and the optimal use of it according to a particular scenario. To this end, this paper comprehensively reviews the methods from both principles and experiments. It is structured as follows: firstly, the imaging models usually used by the HDR 3D techniques are introduced in section 2. Then, in section 3 the equipment-based methods and the algorithm-based methods are explained in theory. Next, in section 4, we present and compare the experimental results obtained with a set of implemented techniques. In section 5, the applicability to different HDR scenarios and the advantages and disadvantages of the reviewed techniques are analyzed. Lastly, in sections 6 and 7, we discuss the future research directions of HDR 3D measurements and conclude the paper.

2. Imaging models

There are two commonly used imaging models for HDR 3D measurements using fringe projection. The first one concentrates on the imaging process of the camera. Assuming the camera sensitivity is s, the exposure time is t, the projected light is I_p, the ambient light is β_1 and β_2 (directly entering the camera), the surface reflectivity is α, and the camera noise is η, the captured fringe image can be expressed by

$$I_c = st\left(\gamma I_p + \gamma\beta_1 + \beta_2\right) + \eta. \quad (1)$$

This model indicates that dark/bright surfaces can be imaged through properly increasing/reducing the exposure time t. However, the limitation of this model is that it implicitly assumes that diffuse reflection dominates during the imaging process.

One the other hand, the second imaging model aims at analyzing the reflection process [82]. The model shows that the surface radiance is comprised of three primary reflection components: the diffuse lobe, the specular lobe, and the specular spike. The diffuse lobe represents the internal scattering mechanism and is distributed hemispherically in all directions. The specular lobe represents a single reflection of incident light. It tends to be distributed around the specular direction and has off-specular peaks. The specular spike represents mirror-like reflection and is concentrated in a small region around the specular reflection. The radiance of the surface in the camera direction is the sum of the three components. This model implies one can remove the specularity by changing the position of the camera or separating the specular reflection components from the overall radiance.

3. Strategies of HDR 3D measurements with fringe projection

We divide the various fringe projection techniques developed for HDR 3D measurements into two groups: equipment-based techniques and algorithm-based techniques. The equipment-based approaches are further divided into camera-based techniques, projector-based techniques, additional equipment-based techniques, and hybrid techniques.

3.1. Camera-based techniques

As can be seen from equation (1), a reduced exposure time is suitable for bright areas, and a long exposure is appropriate for dark surfaces. With this idea, Zhang and Yau [46] proposed to project a set of fringe images which are captured at several times with different exposures. Then, the images are fused into new patterns where fringes with the highest but unsaturated intensity are retained for different parts of the surfaces. This approach is easy to implement. Qi *et al* [47] utilized the camera multi-exposure strategy and presented a method to improve the quality of the captured patterns, where the issues of saturation and low contrast can be solved. However, the multiexposure strategy is sensitive to the ambient light which can affect the image fusion. Also, the selection of the exposure time is empirical and normally many exposure times are required to realize the HDR measurements. To remove the influence of the ambient light and the noise, Long *et al* [48] suggested a new saturation detector that is the non-principal frequency component. This detector is more sensitive and robust in identifying the image saturation than the traditional one searching for the highest intensity. To reduce the number of exposures, approaches in [49, 70] suggested obtaining pre-knowledge of the scenario by calculating a histogram of it, by which the HDR scenarios can be measured with several exposure times predicted. To further improve the measurement efficiency and remove human intervention, techniques reported in [50, 51] can automatically estimate a global optimal exposure time according to the measured objects. But, the unique exposure time is estimated according to the brightest area of the scenario, which makes it difficult for the system to perceive details of dark objects in the scenario. To deal with this problem, Rao and Da [52] presented a method which can automatically predict several optimum exposure times for unknown scenarios by using the histogram of fringe modulation. However, the total number of exposures tends to be fixed as five in this method, which makes the measurement less flexible.

The above multi-exposure techniques use sinusoidal patterns to obtain the phase and then convert it into 3D shapes. However, phase calculation with sinusoidal patterns is sensitive to specular reflection and abrupt variation of texture. Therefore, instead of analyzing sinusoidal fringes, Song *et al* [53] suggested detecting the edges of binary patterns to recover the profiles of shiny objects. Benefitting from multi-exposure, the method calculates HDR fringe images from estimated radiance maps in which the saturation is relieved. Practically, shiny objects can also be measured without tuning the exposure time. Feng *et al* [54] presented a dual-camera fringe projection system to measure reflective objects. The idea is that if one camera is saturated, the other one can be used to compensate the saturation error since the two cameras viewing from different angles are not likely to be saturated at the same time. Therefore, they can mutually compensate for the measurement of the whole scenario. However, the method tends to compromise when handling scenarios where both shiny and dark surfaces are present, since it is difficult to capture the dark area with improved quality just be changing the camera position.

3.2. Projector-based techniques

The previous section introduces methods which employ a strategy of changing the exposure time or adjusting the camera viewpoint to capture the light intensity for an HDR scenario. Actually, one can also change the brightness of the projected light I_p to capture desired images as indicated by equation (1). The maximum input gray level (MIGL) is a commonly used parameter to control the intensity of the projected image. It was first introduced by Waddington and Kofman [55] who they suggested that HDR fringe images can be synthesized by combining the intensities from images captured at different MIGLs. This strategy can be thought of as an inverse multi-exposure technique. However, since this technique can only adjust the projected intensity homogeneously for the whole image, one has to project many images to produce a composite image, which could be time-consuming. The same group presented a modified MIGL method which can calculate a global MIGL for the whole scenario considering the ambient light [56]. This method can save the number of projections but is subjected to a limited dynamic range. Zhang *et al* [57] presented a technique which can predict several proper MIGLs for surfaces with a wide range of reflectivity. By estimating the intensity response function of the camera and calibrating the reflectivity of the measured scenarios, the required MIGLs can be adaptively calculated.

To further reduce the number of projected patterns, methods in [58–61] introduced adaptive fringe-pattern projection methods. With the calibration of reflectance, the MIGL can be modified locally in each projected fringe pattern according to the illuminance required for the different surfaces. As the methods can estimate the MIGL adaptively for surfaces with different reflectivity, they can measure HDR scenarios with only one set of modified patterns. It is noted that the mapping from the camera pixels to the projector pixels is important to these adaptive methods, since the projector needs to use the camera to 'see' where the saturation is and then adjusts the MIGL for the corresponding pixels. Practically, the mapping is implemented using the phase information or the homography matrix. For flat and smooth surfaces, both of them can be applied. For objects with complex shapes, however, the mapping exploiting the phase information is more favorable, since it is insensitive to the geometric variation. In the procedure of changing the local MIGL, the difference in the resolution and field of view between camera and projector can also cause errors. To cope with this issue, Chen *et al* [62] presented a method to further adjust the MIGL of modified patterns according to the feedback of real captured images. Aside from tuning the MIGL, approaches recursively adjusting projected images pixel by pixel based on the reflected images were presented [63, 64]. The advantage is that human intervention is avoided, since the methods do not need the calibration of reflectance. However, relatively complex algorithms are involved to update the projected images. In addition, Qi *et al* [65] proposed a highlight removal method with the projection of region-adaptive patterns, by which the profile of glossy areas is measured with the assists of their neighboring unsaturated points. This method assumes smooth surfaces, and thus will be subjected to geometrically complex objects.

3.3. Additional equipment-based techniques

In addition to adjusting the parameters of the camera or the projector, one can also resort to additional equipment to capture optimal fringes. Ri *et al* [66] presented an intensity range extension method using a self-developed digital micro-mirror device (DMD) camera. As the camera captures images which are reflected by the DMD, users can increase or decrease the captured intensity through manipulation of the DMD. But, practically, it is not easy to accurately align the pixel of the charge-coupled device with the corresponding micro-mirror of the DMD. As indicated by the second imaging model in section 2, saturation can be avoided if one can separate the specular components from the overall captured intensity. It is well known that a significant character of specular reflection compared with diffuse reflection is that it is usually much more strongly polarized. Thus, the separation can be realized with the consideration of their difference in polarization. With this idea, Chen *et al* [67] proposed polarization-difference imaging to scan translucent and shiny objects. By introducing two linear polarizers, one of which is employed to polarize the projected light and the other is to polarize the captured light, the highlight intensity can be removed when their axes are oriented perpendicularly. Although saturation is avoided, the signal-to-noise ratio (SNR) of the whole scenario is reduced at the same time due to the attenuation caused by the polarizers. Compared with Chen's method, Salahieh *et al* [68] proposed a similar but more robust 3D imaging method by replacing the ordinary camera with a polarization camera. One of the polarized channels can be used to retrieve shiny surfaces while other channels can be selected to enhance the fringe contrast for the other areas. However, the spatial resolution of the recovered 3D points is limited due to the spatial multiplexing in the polarization camera. Moreover, Cai *et al* [69] presented a multidirectional depth estimation framework using a light field camera. Since the light field camera can simultaneously record the position and direction of incoming light rays, it can be thought of as many cameras which are measuring the scenario with different viewing positions. However, the bottleneck of light field imaging is the image resolution, which will restrict the quality of reconstructed 3D results.

3.4. Hybrid techniques

In the bibliography, there are some methods which rely on the modification of camera exposure but also take into account other strategies, e.g. introducing additional equipment, changing the viewing position, or adjusting parameters of the system. As mentioned in the last subsection, the method of introducing polarizers for the camera and the projector can remove the highlight intensity on shiny surfaces [67], but it is fragile for low-reflective surfaces as the polarizers would inherently attenuate the captured intensity. To handle this problem, Feng *et al* [70] combined the idea of multi-exposure with the strategy of polarization and proposed a general framework for HDR measurements. As increasing the exposure time of the camera is beneficial to capturing fringe patterns on dark surfaces, this method is applicable for scenarios containing both high- and low-reflective objects. In addition, different from the traditional method of multi-exposure where the exposure time is predicted empirically, this method can estimate the optimal exposure time adaptively according to the statistic distribution of the reflectivity of the scenario. Alternatively, Liu *et al* [71] found that points corresponding to highly specular or dark areas can survive in the traditional multi-exposure technique. The authors suggested combining the strategies of the dual-camera set-up and the multi-exposure strategy to correct the inaccurate points. Moreover, Jiang *et al* [72] presented a hybrid method to capture optimal fringe patterns by not only adjusting the exposure time of the camera but also changing the projected intensity of the projector. This method is more robust than the traditional multi-exposure technique, since it not only enables adjustments of the camera and projector simultaneously, but also adopts fringe modulation as the criterion to select optimal patterns in image fusion, which is less sensitive to the influence of ambient light. However, the method usually measures a scenario by adding at least five times the number of projecting images compared to the normal phase measurement, which limits its efficiency. For rapid *in situ* measurements, the same group proposed a fast HDR solution [73], in which a high-speed projector is used to project intensity-varying fringe images at 700 Hz. As a result, the measurement time cost can be saved.

3.5. Algorithm-based techniques

Different from the methods mentioned above, the techniques in this group try to calculate 3D reconstructions from saturated fringe images. They are especially useful when the adjustment of the camera or the projector is not allowed, or additional equipment is not available. Yin *et al* [74] suggested measuring shiny surfaces with a single color image. The authors found that due to the wavelength selectivity of the Bayer filter in a color camera, the R/G/B channels have different quantum-efficiency responses (different captured intensity) to the input wavelength. Therefore, the images from different channels can be synthesized for HDR imaging. However, the method may be fragile for surfaces with chromatic textures, since the inherent color of objects tends to change the captured images. Moreover, Jiang *et al* [75] proposed a real-time HDR 3D scanning method by projecting additional inverted fringe patterns. The idea is that when both original and inverted fringe images are used, the inverted patterns can be used to complement the pixels with the highlight intensity of the original images. However, one has to use different functions for the phase calculation according to the number of saturated images. As this method lacks a universal solution, Wang *et al* [76] introduced an enhanced method using the generalized phase-shifting algorithm, which also projects inverted patterns but can calculate the phase in a generic framework which utilizes all of the unsaturated gray values to compute the phase.

Chen *et al* [77] and Hu *et al* [78] found the image saturation can be overcome if the phase shift is high enough to obtain at least three unsaturated fringe intensities for the phase estimation. For these techniques, however, the different phase-shifting algorithms will correspond to entirely different calculations of the phase, thus increasing the complexity of its implementation. Without considering whether images are saturated or not, Chen *et al* [79] suggested calculating the phase from saturated phase-shifting patterns. However, since the phase shift is determined according to the fringe period, one needs to capture a large number of phase-shift images when wide stripes are used, which can be time-consuming and laborious. It is noted that the approaches in [77–79] are benefitting from an increased phase shift. Actually, the phase distortion caused by the saturation can be corrected effectively even with the standard N-step phase-shifting algorithm as long as the phase shift is large enough [80]. With trigonometric properties, the phase error due to saturation can be derived as

$$\Delta\phi = \arctan \frac{\sum_{i=1}^{N} {I'}_i \sin\left(\phi + \frac{2\pi i}{N}\right)}{\sum_{i=1}^{N} {I'}_i \cos\left(\phi + \frac{2\pi i}{N}\right)} \quad (2)$$

where $\Delta\phi$ is the difference between the measured phase and the true phase, ϕ is the true phase, and ${I_i}'(x, y)$ is the captured image with

$${I_i}'(x, y) = \begin{cases} I_i(x, y) & \text{if } I_i(x, y) \leqslant I_{\max} \\ I_{\max} & \text{if } I_i(x, y) > I_{\max} \end{cases} \quad (3)$$

where I_i is the actual intensity and $I_{\max}$ the maximum allowed intensity of a sensor, e.g. 255 for an 8-bit sensor. We simulate a reflective surface to show the performance of phase-shifting algorithms on the correction of the phase error. In the simulation, the maximum intensity of the fringe image is triple the

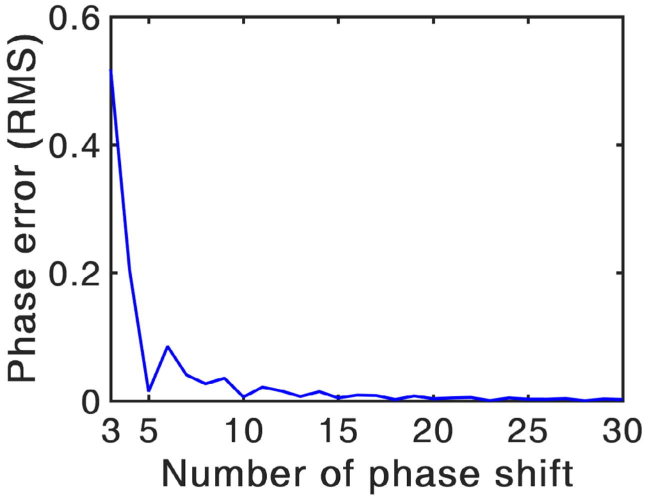

Figure 2. Phase error correction by the *N*-step phase-shifting algorithm in simulation.

upper limit of the dynamic range. Figure 2 shows the root mean square phase error of the phase-shifting algorithm. We can see that the phase error reduces sharply with the increase in phase shift. For the phase-shifting method with the minimum phase shift ($N = 3$), the error is 0.5167 rad. When the phase shift rises to 30, the error is cut down to 0.0022 rad, which shows the accuracy has been improved by 99.57%. Recently, Qi *et al* [81] introduced a theory to analyze this saturation-induced phase error from the viewpoint of digital signal processing. They found that the phase error is the result of the non-integer-period sampling that exists in the capture of saturated phase-shifting fringes and suggested the seven-step phase-shifting algorithm to be applied when the saturation is not significant. It is noted that the saturation issue discussed here is mainly caused by diffuse reflection. For the case where specular reflection is dominant, the alleviation will not be significant even with a large phase shift, which will be demonstrated by our experiments.

4. Experimental results

We implemented a set of six representative techniques taken from the proposed classification groups. All the techniques were tested under the same conditions to evaluate their performance. For comparison, we exploited the three-step phase-shifting algorithm with fixed exposure time and projected intensity to calculate the original 3D reconstruction. In the experiments, the fringe projection system consists of a DLP projector (LightCrafter 4500, TI) and a high-speed industrial camera (acA640-750, Basler). The resolution of the projector was 912 × 1140, and that of the camera was 640 × 480. To remove the effect of gamma distortion, we chose equipment that is manufactured without gamma coding. A laptop (Lenovo Y430P) was used to carry out the calculations.

All the experiments were conducted in a dark room, i.e. we switched off the lights to reduce the effect of ambient light. In the implemented techniques, we exploited three sets of three-step phase-shifting fringe images to retrieve the phase. The frequencies of each set of images were 1, 8, and 80 respectively. Thus a temporal phase-unwrapping algorithm followed to recover unambiguous phase distributions [83–85]. We calibrated the camera and the projector in advance and calculated 3D point clouds by treating the projector as an inverse camera [86–88]. The settings of the camera or the projector were determined from a set of parameters, e.g. exposure time, projected light intensity, and so on, thus constituting just a sample of the selected methods. The purpose of the experimental results was to compare each technique concerning the others rather than going deep into the details of providing the optimal parameters that depend on measured surfaces. It is noted that some methods require changing the exposure time and the projected light intensity in theory. Thus, for the rest of the techniques without explicit statement, the exposure time was fixed at 39 ms, and the maximum projected light intensity as 255. From each group we selected at least one technique, and the implemented techniques are listed below.

- Camera-based techniques.

Zhang: Every fringe image was projected at a fixed illuminating period of 8.5 ms (the minimum allowed period for an 8-bit pattern with our projector), and was captured with an exposure time of 8.5 ms at the beginning. Then for the followed exposure time, the increment was 8.5 ms, i.e. the exposure time was equal to 8.5 ms, 2 × 8.5 ms, 3 × 8.5 ms and so on. To cover a wide range of variation of reflectivity, the maximum exposure time was 30 × 8.5 ms [46].

- Projector-based techniques.

Li: To calibrate the coefficients of projected patterns, six rounds of pattern projection were implemented. The corresponding maximum input gray levels were 0, 40, 80, 120, 160, and 255 respectively. It is noted that the gray level of 0 was used to predict the image noise [58].

- Additional equipment-based techniques.

Chen: Two linear polarizers with an extinction ratio of 100:1 were put in front of the camera and the projector respectively [67]. The method was simplified for the measurement of shiny surfaces with the axes of the polarizers remaining perpendicular during experiments.

- Hybrid techniques.

Since the hybrid techniques have the combined advantages of more than one method, we chose two representative techniques from this group.

Feng: Analogous to the method of Chen, two linear polarizers with an extinction ratio of 100:1 were put in front of the camera and the projector respectively. For this method, the exposure time to capture the pure white image was 39 ms, which was used to predict the optimal exposure time for the measured objects after the polarizers removed the highlight intensity [70].

Jiang: By this technique, we changed the exposure time of the camera as well as the projected intensity of the projector [72]. The parameters of the camera and the projector are shown in table 1.

Table 1. Parameter settings of Jiang's technique.

Serial number	Projected fringe (average, amplitude)	Exposure time (ms)
1	(25, 25)	39
2	(50, 50)	39
3	(75, 75)	39
4	(100, 100)	39
5	(127.5, 127.5)	39
6	(127.5, 127.5)	78

- Algorithm-based techniques.

Bruning: The 30-step phase-shifting algorithm where the phase shift equals $2\pi/30$ [80].

In the first experiment, we measured a white ceramic vase as shown in figure 3(a). From this experiment, we wanted to see the performance for highly reflective surfaces. From a captured fringe image as shown in figure 3(b), we can see that there are shiny areas on the surface, especially on the bottleneck (Region 1) and the embossment of the vase (Region 2). Figure 3(c) shows that the original method failed to reconstruct the saturated areas correctly. Figure 4 displays the 3D reconstructions of the selected techniques. In general, these approaches successfully measured the shape of the vase but with different performances for shiny local areas. For a detailed comparison, we enlarged the reconstructions of the two regions as can be seen in figures 5 and 6. In figures 5(a)–(g), we show the reconstructed 3D point clouds of Region 1. We can see that the two methods (Chen and Feng) based on polarization outperformed the other techniques. The highlights have been removed completely with the assist of polarizers. But for the rest of the methods, from their reconstructions, it is difficult to observe significant improvements compared with the images obtained by the traditional method.

For Region 2, the calculated 3D reconstructions are shown in figures 6(a)–(g). Again, we can see the polarization-based techniques performed better than the other methods for the embossment with shiny spots. Furthermore, among the techniques based on polarization, the method of Feng obtained a more smooth 3D result than the method of Chen from careful comparison of the results. The reason is that the exposure time of the camera changes for different parts of the vase, which ensures a sufficient SNR of the captured fringe images for different regions. For the other techniques, the reconstructed shiny areas of the embossment can be observed with slightly fewer artifacts through the multi-exposure method of Zhang compared with the other methods.

It is noted that for the techniques of Zhang, Li, and Jiang, the intensity of shiny areas was captured less than 255 through the adjustment of the camera or the projector. But we still failed to retrieve the areas accurately as shown by the results. This experiment indicates that for techniques that are based on the adjustment of the camera and the projector, or that based on a phase-shifting method, it is difficult to overcome the issue of saturation for a highly reflective object. The reason is that when the specular component is dominant, it is difficult to remove its effect by merely adjusting imaging parameters or through the calculation strategy, even though the image is captured without saturation and the phase shift is large enough.

In the second experiment, we measured a more complex scenario that consists of a dark box in the background, a plaster model of David on the left side, a metallic cube in the middle (with a rough surface), and a circular plate on the right side, as shown in figure 7(a). From this experiment, we wanted to see the performance for scenarios with a large variation of reflectivity. From a captured raw fringe image, as shown in figure 7(b), there are under-exposed pixels at the surface of the dark box in the background (1), whereas there are saturated pixels on the surface of the metallic cube (2), the face of David (3), and the left edge of the circular plate (4). From the original 3D reconstruction as shown in figure 7(c), we can observe serious reconstruction errors that occur on the labeled surfaces.

Figure 8 shows the 3D reconstructions of the reviewed techniques. To see the local reconstruction, figure 9 shows the surface of the dark box (1). The original 3D reconstruction displayed in figure 9(a) shows noisy 3D point clouds for the low-reflective surface. Among the selected techniques, we find the polarization-based method of Chen failed to measure the surface, as shown in figure 9(d), because of the reduced SNR of captured fringe images caused by the polarizers. Thus, the pixels with low SNR were treated as outliers and were removed. The method of Li retrieved the geometry of the surface but with a noisy reconstruction. The reason is that the projected fringe patterns are limited to the used digital projector which can only project 256 gray levels from 0 to 255. With a projector of larger pixel depth, this problem would be relieved. The other methods all performed well for the low-reflective surface.

Next, figure 10 shows the reconstructions for the metallic cube (2). Because of the saturation, we can observe significant errors on the surface obtained with the original method, as shown in figure 10(a). Figures 10(b)–(g) show the reconstructed results when the reviewed techniques were implemented and table 2 lists the corresponding reconstruction error (root mean square error) of the surface, which is fitted to a plane. Among the results, significant improvements can be observed with the reviewed techniques except for the one of Chen. The insufficient light intensity of the captured fringes leads to the noisy point cloud retrieved by the method of Chen. On the other hand, Bruning's method shows the highest accuracy among the selected methods owing to the large phase shift.

Next, figure 11 displays the reconstructions of the plaster model of David (3). Although nearly half of the face failed to be measured by the traditional method due to the highlights, noticeable improvements have been made with the selected approaches. Since the plaster model is a diffuse object, the problem of saturation can be solved effectively with the techniques. Finally, figure 12 shows the retrieved point clouds of the circular plate with a small shiny region (4), for which the reconstruction error is listed in table 2. The results indicate that for a reflective surface that is not ideally diffuse, based on the adjustment of the exposure and the projected intensity

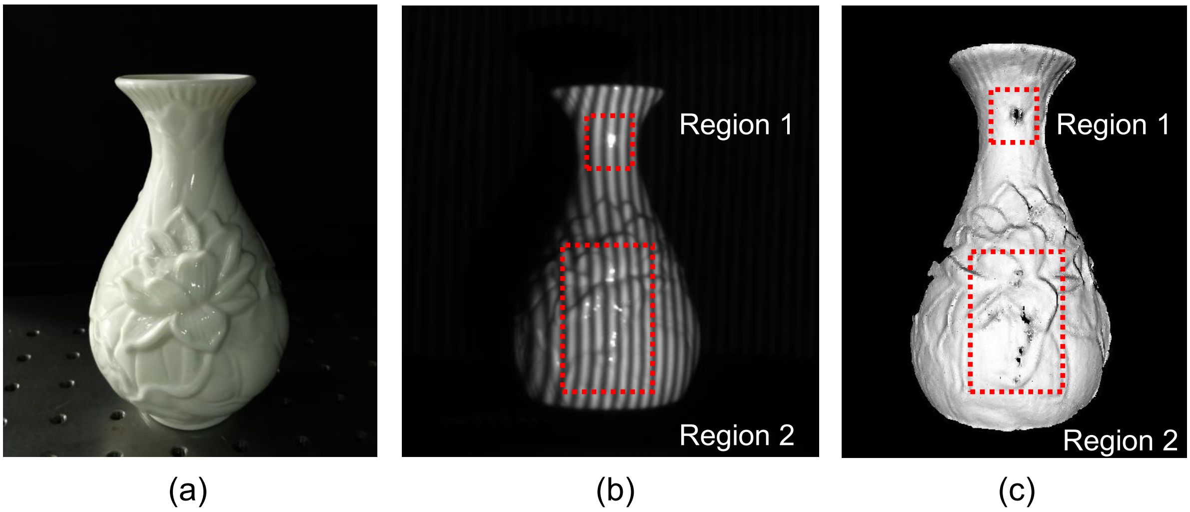

Figure 3. The measured object in the first experiment. (a) The ceramic vase; (b) one of the raw fringe images; (c) the original 3D reconstruction.

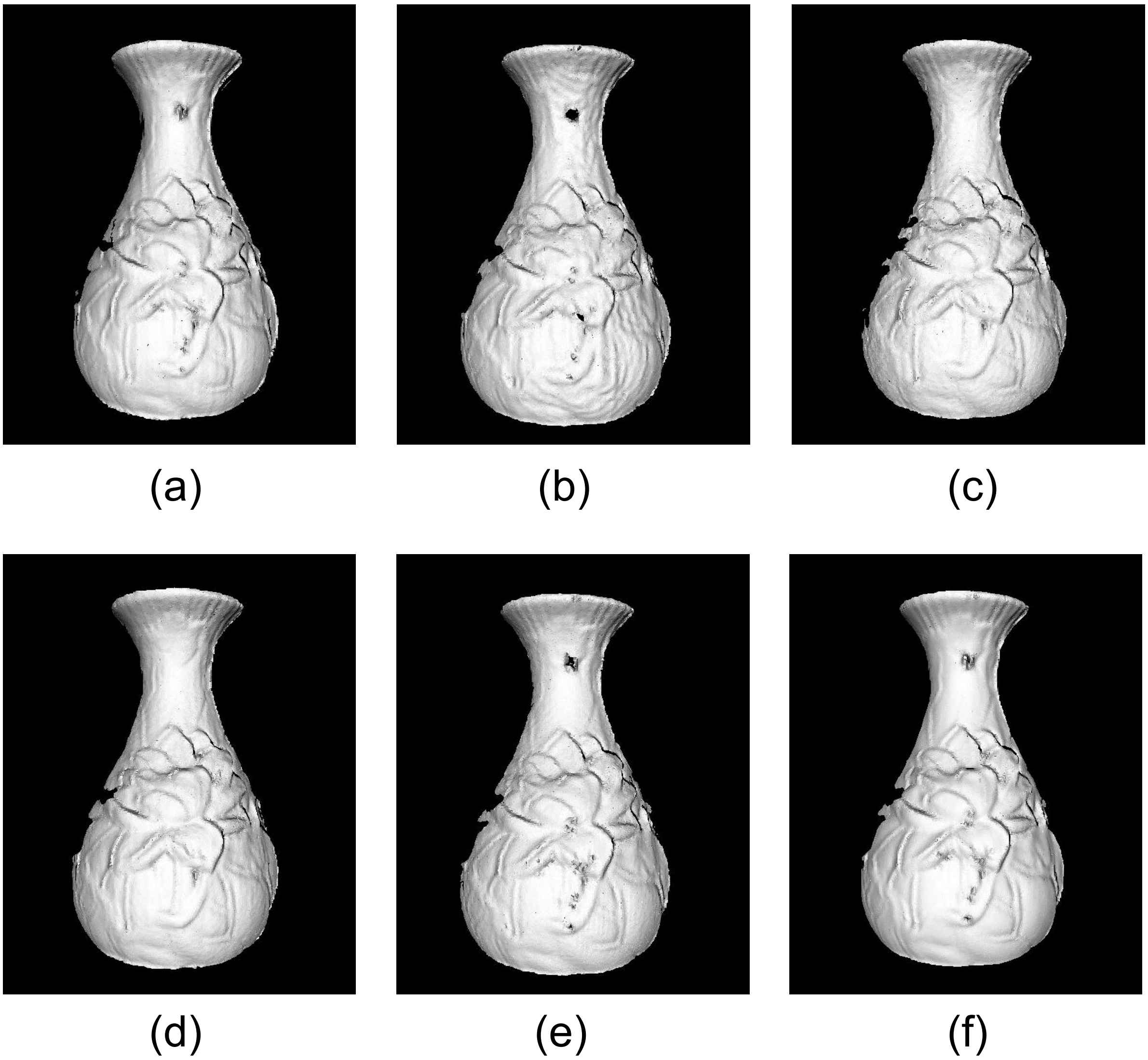

Figure 4. The 3D reconstructions. (a) Zhang; (b) Li; (c) Chen; (d) Feng; (e) Jiang; (f) Bruning.

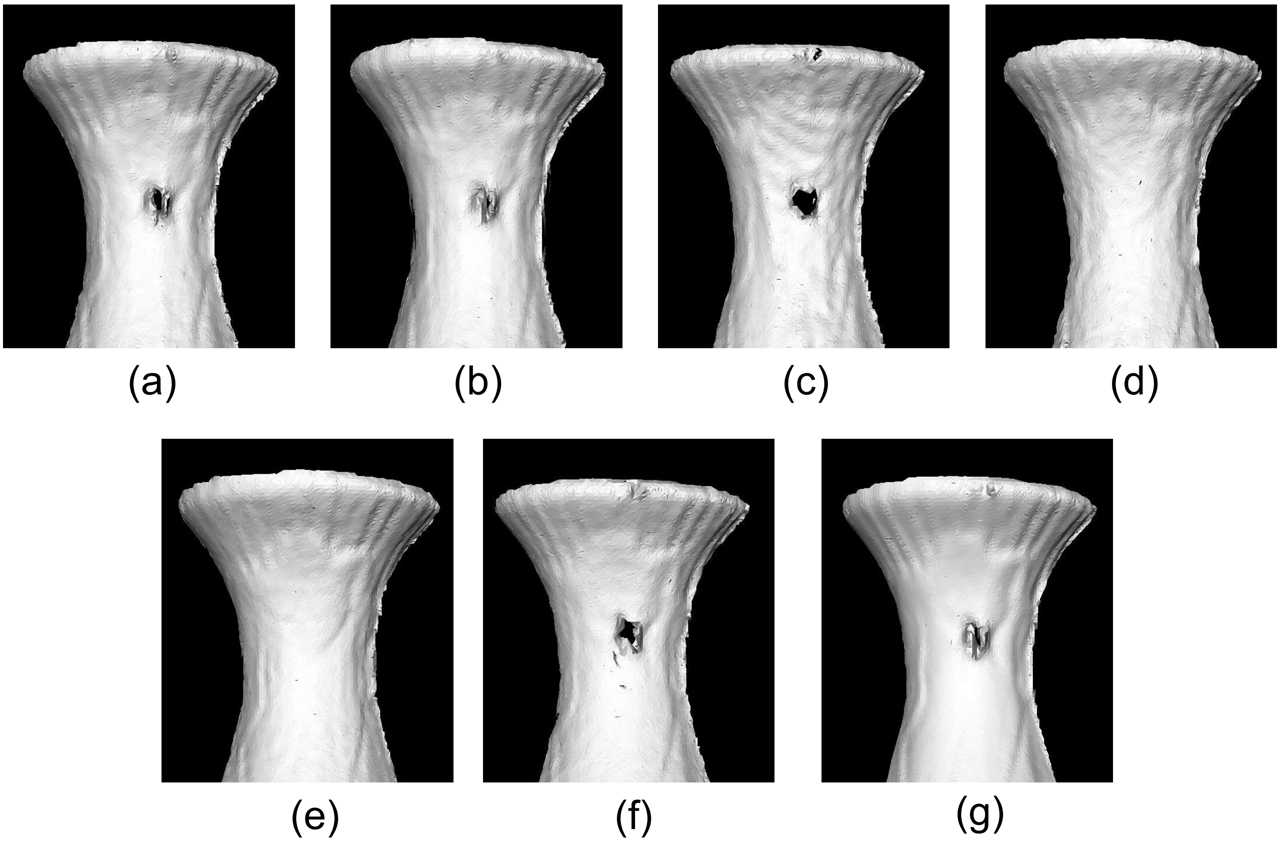

Figure 5. The 3D reconstructions of Region 1. (a) Original; (b) Zhang; (c) Li; (d) Chen; (e) Feng; (f) Jiang; (g) Bruning.

or the phase-shifting algorithm, the techniques can mitigate the effect of saturation to some extent but have difficulty in removing it entirely. However, the methods of Chen and Feng, with the assist of polarizers, can eliminate the saturation successfully and reconstruct the shiny area with higher accuracy. Among them, Feng's method achieved higher precision than that of Chen as the former compensated for the light intensity of captured images attenuated by the polarizers. Also, we can observe that there are some grid artifacts on the surface calculated by Li's method. The reason is that the camera pixels did not strictly align to the projector pixels for the corresponding region.

5. Discussion

5.1. Comparison of applicability

To compare the applicability of all of the reviewed techniques, we select four different HDR scenarios as follows.

Scene 1: There are only shiny areas where the saturation is caused mainly by diffuse reflection.

Scene 2: There are dark surfaces and shiny areas where the saturation is caused mainly by diffuse reflection.

Scene 3: There are only shiny areas where the saturation is caused mainly by specular reflection.

Scene 4: There are dark surfaces and shiny areas where the saturation is caused mainly by specular reflection.

The result is shown in figure 13. We can see that all of the reviewed methods can deal with the saturation caused by diffuse reflection in Scene 1. For Scene 2, although most of them are still applicable [46–81], some techniques tend to fail for measurements of dark surfaces [50–78]. This is because they use only a single exposure or are developed specially for shiny objects which may not be able to cover a wide range of reflectivity. Next, for Scene 3, only a few methods can handle the saturation problem caused by specular reflection. The reason is that the most of the reviewed techniques depend on the phase-shifting method which requires diffuse reflection. The effect of specular reflection cannot be simply removed even if the images are captured with seemingly correct intensity through the change of exposure or brightness of projection. By contrast, more appropriate methods are those exploiting the separation of the specular reflection, multi-view geometry or binary patterns [53, 54, 61, 65, 67–71]. Finally, Scene 4 seems to be the most difficult one to handle, since there are only five reviewed techniques which can deal with the saturation caused by specular reflection and the low SNR signal on dark surfaces [53, 61, 69–71]. Among them, two methods use compensated binary patterns [53, 61]. One removes the specularity by the polarizers and compensates for the signal on dark surfaces by camera multi-exposure [70], and the rest resort to the multi-view geometry together with selection of proper exposure time [69, 71]. In summary, for the overall evaluation, there are five techniques which have the highest applicability to different surfaces [53, 61, 69–71] and most of the reviewed

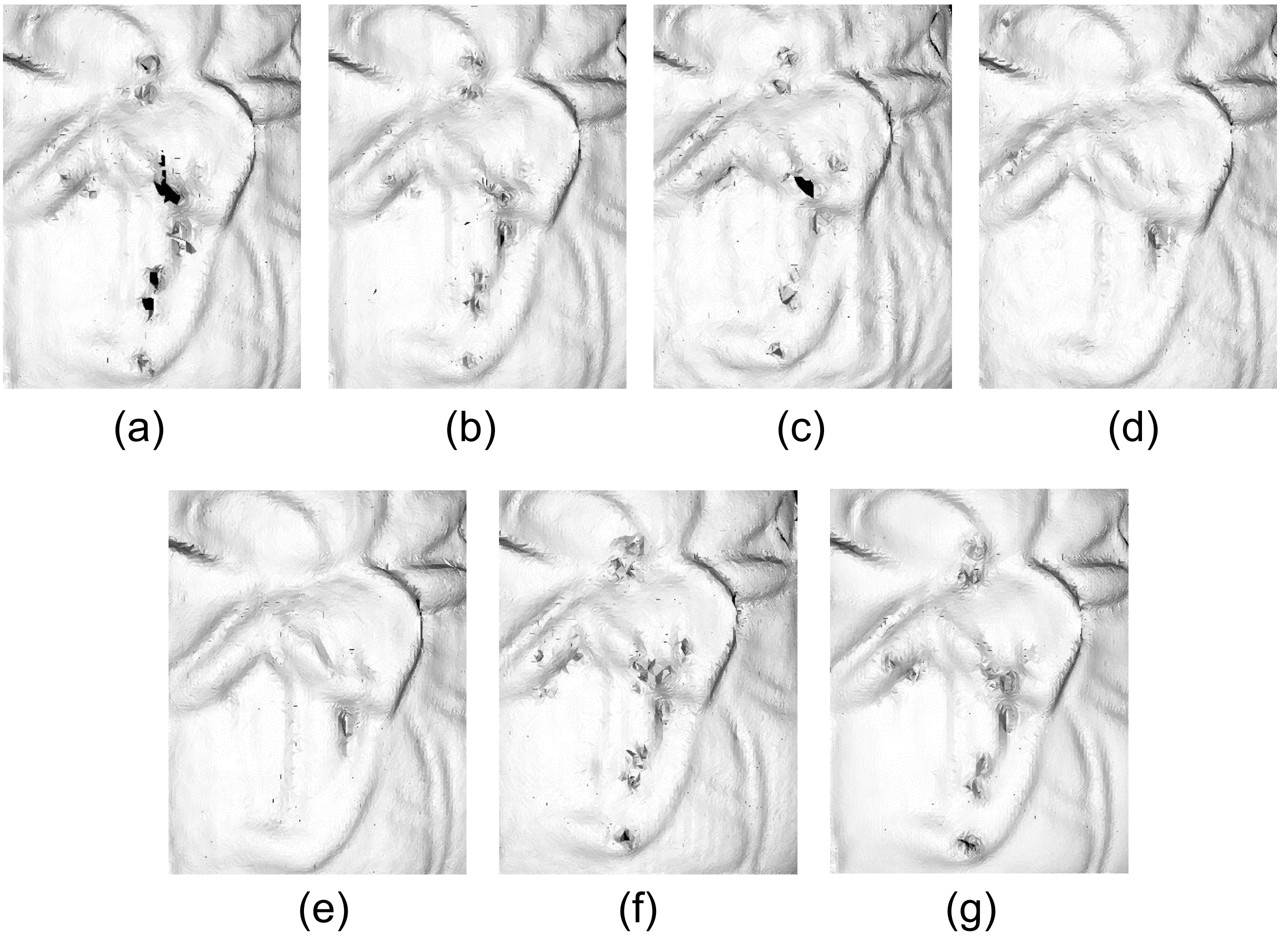

Figure 6. The 3D reconstructions of Region 2. (a) Original; (b) Zhang; (c) Li; (d) Chen; (e) Feng; (f) Jiang; (g) Bruning.

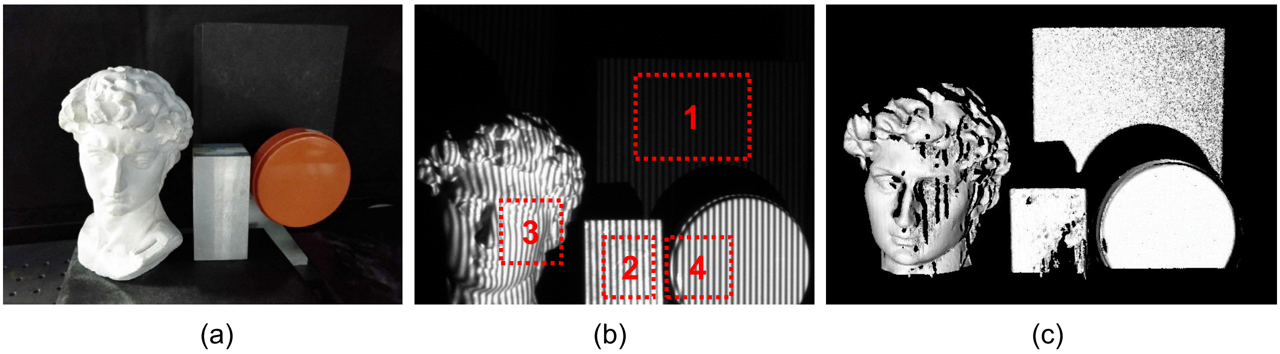

Figure 7. The second experiment. (a) A complex scenario; (b) one of the raw fringe images; (c) the original 3D reconstruction.

techniques can handle HDR scenarios with dark surfaces and diffusely reflective objects.

5.2. Advantages and disadvantages

We discuss the reviewed techniques from six different aspects to show their advantages and disadvantages. They are evaluated according to the complexity of the measuring system, the complexity of the algorithm, the number of measurements, the auto-selection of parameters, the ability to resist the effect of ambient illumination, and the potential for the measurement of moving objects. The results are shown in figure 14. First, the complexity of the measuring systems is compared. The simpler the system, the more stars it obtains. It should be noted that although the techniques may be implemented with slightly different set-up, the evaluation is carried out based on the systems reported. Systems that can be built using the simplest arrangement, i.e. a projector and a camera, receive three stars. We can see that most of the reviewed techniques use this arrangement [46–48, 50, 52, 53, 55–61, 63–65, 68, 69, 74–81]. For the methods with two stars [49, 51, 54, 62, 67, 70–73], the systems are built with more than one camera or using additional equipment. Thus, the complexity is increased slightly. The system suggested by [66] is more complex than the rest, since it requires additional precise mechanical systems to align the pixels of the camera with those of the DMD.

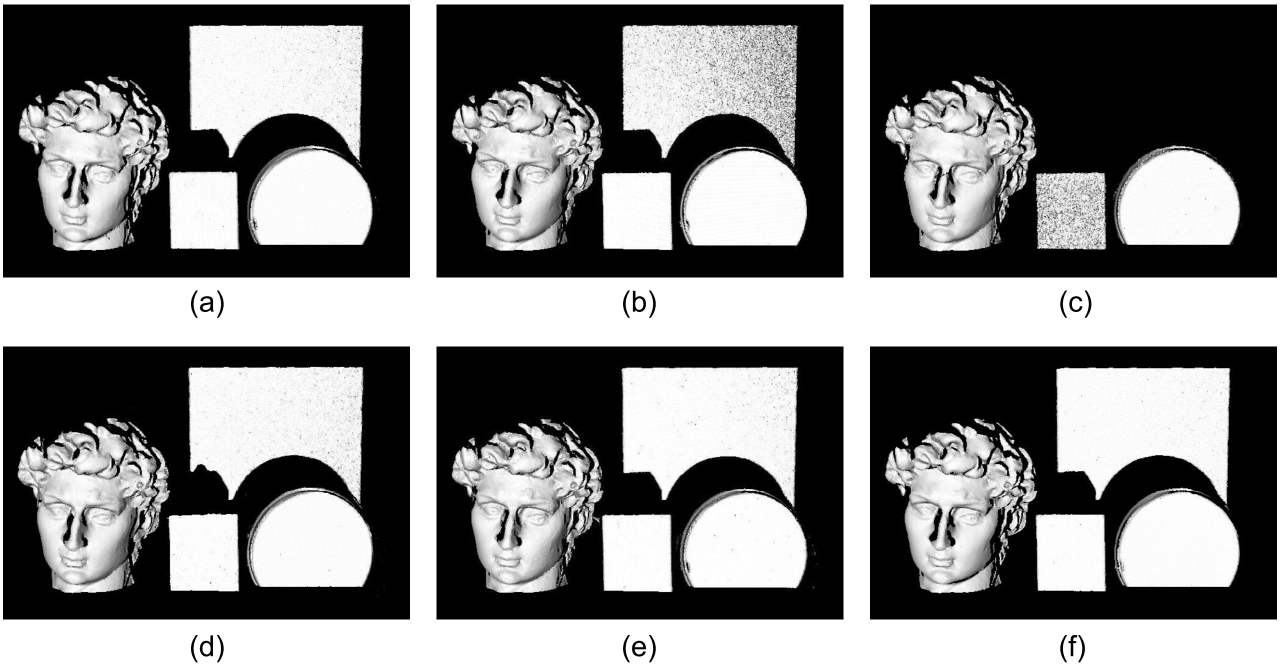

Figure 8. The 3D reconstructions. (a) Zhang; (b) Li; (c) Chen; (d) Feng; (e) Jiang; (f) Bruning.

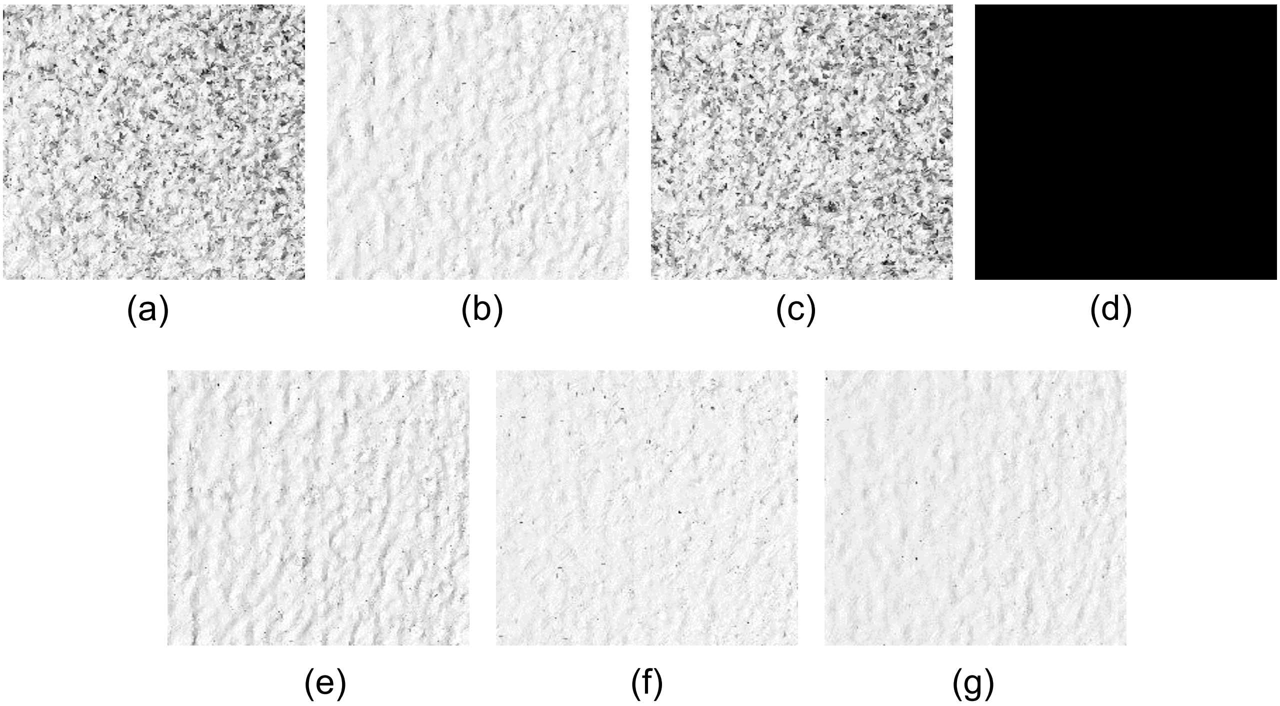

Figure 9. The enlarged view of the 3D reconstruction of the dark box. (a) Original; (b) Zhang; (c) Li; (d) Chen; (e) Feng; (f) Jiang; (g) Bruning.

Then, we compare the complexity in algorithms. The lower the complexity, the more stars the method acquires. From figure 14, there are five approaches having three stars [66, 67, 79–81]. This is because they only rely on standard phase-shifting algorithms to realize HDR 3D measurements. For the two-star methods [46–48, 50–52, 55–57, 59, 62, 68, 70, 72–78], some of them need to generate HDR fringe images by capturing raw images with different exposure times or brightness of projection. The others have sophisticated demodulation algorithms. Therefore, they are more complex than the three-star methods. The methods with one star [49, 53, 54, 58, 60–64, 65, 69, 71], use similar ideas to extend the dynamic range to the two-star methods, but they are implemented with algorithms of higher complexity, e.g. through nonlinear fitting, iterations, image correlation, and so on.

Next, we compare the required number of measurements. The fewer the measurements, the higher the efficiency, and thus the more stars the method obtains. With the need for

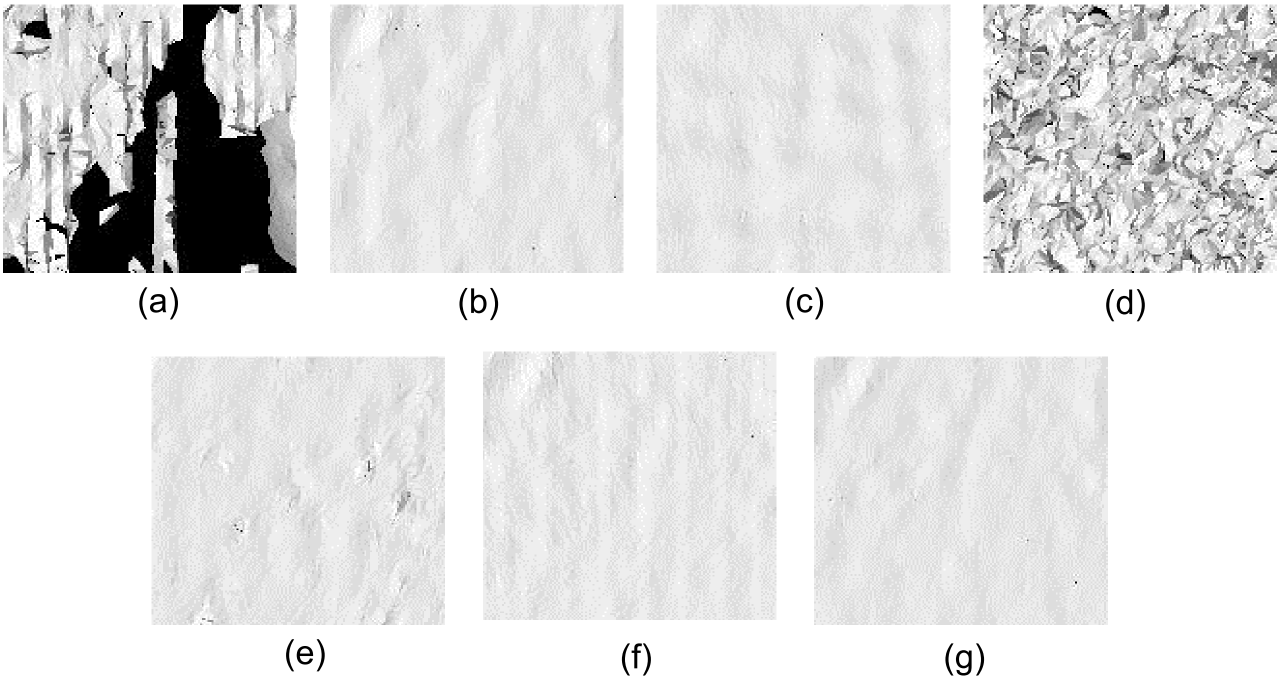

Figure 10. The enlarged view of the 3D reconstruction of the metallic cube. (a) Original; (b) Zhang; (c) Li; (d) Chen; (e) Feng; (f) Jiang; (g) Bruning.

Table 2. Reconstruction error of the implemented techniques.

Technique	Metallic cube (mm)	Circular plate (mm)
Zhang	0.074	0.24
Li	0.088	0.20
Chen	0.34	0.16
Feng	0.073	0.12
Jiang	0.097	0.25
Bruning	0.049	0.22

multiple exposures, changes in the brightness of projection, or the calibration of reflectance, the methods with one star have to measure the scenarios many times [46–48, 50, 51, 53, 55–57, 59–61, 72]. The techniques with two stars [49, 52, 58, 62–66, 70, 71, 73] use similar procedures to the one-star methods, but they can reduce the number of measurements to several times with certain techniques. Thus, the HDR scenarios can be measured with higher efficiency. Lastly, for the three-star methods [54, 67–69, 74–81], we find most of them are additional equipment-based and algorithm-based methods. Due to the assists from the additional equipment or their ability to handle raw images, a single measurement is sufficient for HDR 3D measurements for these techniques.

Also, we discuss the ability to select parameters without human intervention, e.g. the optimal exposure time or the proper brightness of image projection. For an unknown scenario, the ability of auto-selection will avoid aimless attempts using different parameters and thus is important for the efficiency. In the evaluation, the higher the degree of automation, the more stars the method can acquire. From figure 14, the methods [46–48, 53, 55, 71, 73] received one star. The reason is that the parameters are determined mainly through the user's subjective experience. Therefore, the parameters may be selected blindly and laboriously. For the two-star techniques [49–52, 56–66, 70, 72], the optimal parameters can be predicted through the calibration of reflectance or iterations, thus reducing human intervention and showing a higher degree of automation. For the three-star techniques [54, 67–69, 74–81], it is not necessary to change the camera exposure or the projected patterns during the measurement. Therefore, human intervention can be avoided completely. It is noted that most of them are also additional equipment-based and algorithm-based methods.

Furthermore, the ability to resist ambient illumination is discussed. The more powerful the resistance, the more stars the method obtains. For the techniques using image fusion, the ambient illumination will violate the captured intensity, making the selected highest unsaturated intensity unreliable. Moreover, the presence of ambient light also reduces the SNR of captured fringes from dark surfaces. For these reasons, the methods in [46, 47, 49, 50, 52, 54, 55, 67–71] are sensitive to ambient light and thus are given one star. The two-star methods [48, 51, 53, 56–66, 72–75, 77, 78] can calibrate the ambient light or use fringe modulation as criteria for HDR image fusion, and thus are insensitive to ambient illumination. The methods with three stars [65, 76, 79–81] have the most powerful resistance to ambient light owing to the advantage of a large phase shift.

Finally, we investigate the potential for HDR 3D measurement of moving objects. The higher the insensitivity to movement, the more stars the technique receives. We can see that most of the reviewed methods have only one star, which means they are not appropriate for dynamic objects [46–53, 55–66, 70–72, 79, 80]. The reason is that the motion can easily violate the obtained pre-knowledge of the scenario, or the fusion of HDR fringe patterns. The two-star techniques [73, 76, 78, 81] capture fewer images for measurements, and thus are less

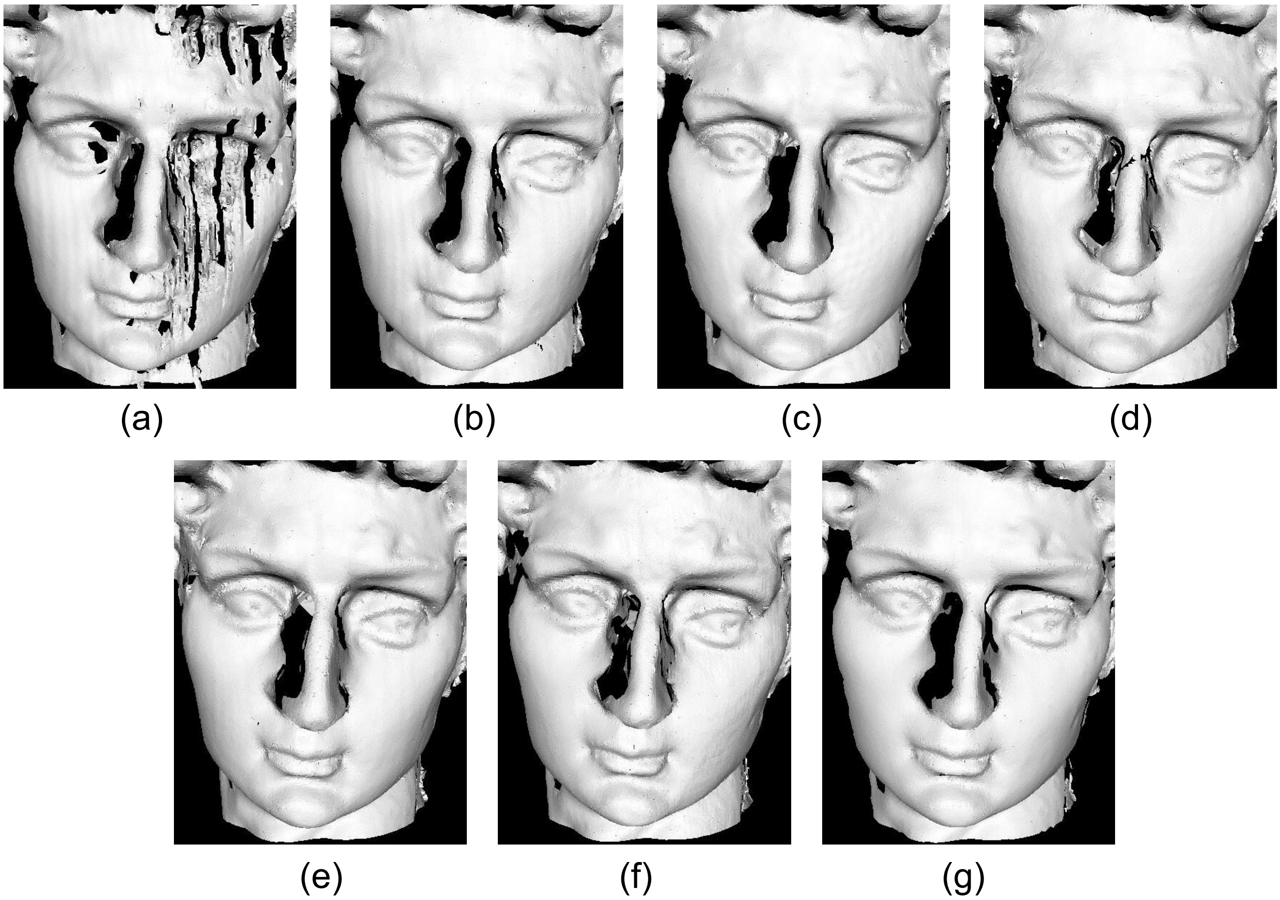

Figure 11. The enlarged view of the 3D reconstruction of the plaster model. (a) Original; (b) Zhang; (c) Li; (d) Chen; (e) Feng; (f) Jiang; (g) Bruning.

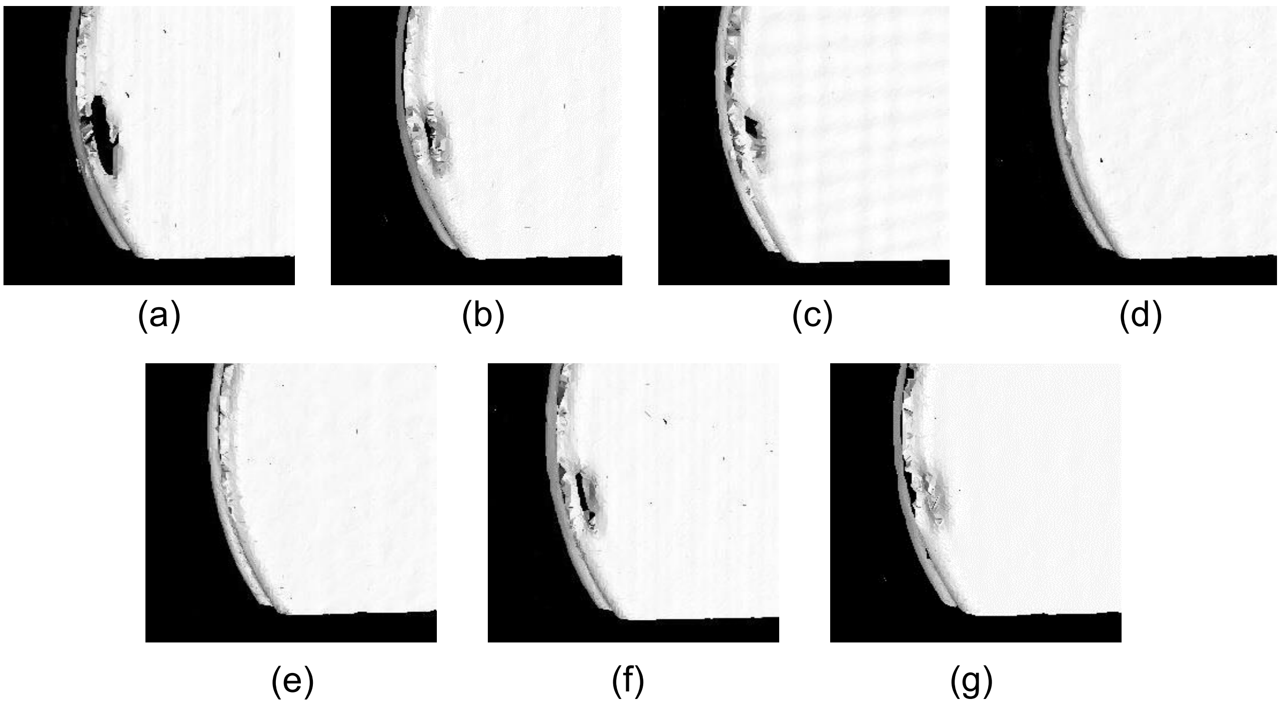

Figure 12. The enlarged view of the 3D reconstruction of the circular plate's left boundary. (a) Original; (b) Zhang; (c) Li; (d) Chen; (e) Feng; (f) Jiang; (g) Bruning.

Scene No.	Features	Suitable techniques
1	Saturation caused by diffuse reflection	All of them
2	Saturation caused by diffuse reflection + Dark surfaces	[46], [47], [48], [49], [52], [53], [55], [57], [58], [59], [60], [61], [62], [63], [66], [69], [70], [71], [72], [73], [74], [79], [80], [81]
3	Saturation caused by specular reflection	[53], [54], [61], [65], [67], [68], [69], [70], [71]
4	Saturation caused by specular reflection + Dark surfaces	[53], [61], [69], [70], [71]

Figure 13. Comparison of the applicability.

Stars	Complexity of measuring system	Complexity of algorithm	Number of measurements	Auto-selection of parameters	Resistance to ambient light	Potential for moving objects
★★★	[46], [47], [48], [50], [52], [53], [55], [56], [57], [58], [59], [60], [61], [63], [64], [65], [68], [69], [74], [75], [76], [77], [78], [79], [80], [81]	[66], [67], [79], [80], [81]	[54], [67], [68], [69], [74], [75], [76], [77], [78], [79], [80], [81]	[54], [67], [68], [69], [74], [75], [76], [77], [78], [79], [80], [81]	[65], [76], [79], [80], [81]	[54], [67], [68], [69], [74], [75], [77]
★★	[49], [51], [54], [62], [67], [70], [71], [72], [73]	[46], [47], [48], [50], [51], [52], [55], [56], [57], [59], [62], [68], [70], [72], [73], [74], [75], [76], [77], [78]	[49], [52], [58], [62], [63], [64], [65], [66], [70], [71], [73]	[49], [50], [51], [52], [56], [57], [58], [59], [60], [61], [62], [63], [64], [65], [66], [70], [72]	[48], [51], [53], [56], [57], [58], [59], [60], [61], [62], [63], [64], [66], [72], [73], [74], [75], [77], [78]	[73], [76], [78], [81]
★	[66]	[49], [53], [54], [58], [60], [61], [63], [64], [65], [69], [71]	[46], [47], [48], [50], [51], [53], [55], [56], [57], [59], [61], [60], [72]	[46], [47], [48], [53], [55], [71], [73]	[46], [47], [49], [50], [52], [54], [55], [67], [68], [69], [70], [71]	[46], [47], [48], [49], [50], [51], [52], [53], [55], [56], [57], [58], [59], [60], [61], [62], [63], [64], [65], [66], [70], [71], [72], [79], [80]

Figure 14. Comparison of advantages and disadvantages. The more stars given, the more powerful the technique.

sensitive to the movement. For the methods having three stars [54, 67–69, 74, 75, 77], only a few images are required, e.g. [54] can measure shiny and discontinuous surfaces with only four images. Therefore, they are more suitable for measurements of moving HDR objects.

6. Future research directions and recommendations

Compared with traditional FPP techniques, HDR FPP techniques show the advantage of higher measurement adaptability to different kinds of surfaces. But, this does not mean that the HDR techniques are trouble-free all the time. First, challenges from measured objects and practical implementation are discussed here. Then, several potential applications for the HDR techniques are introduced. Finally, some measures for better performance are also recommended.

6.1. Challenges from measured objects

6.1.1. Extremely smooth surfaces. For very smooth or mirror-like surfaces, the reflected light will be almost entirely comprised of specular reflection. From our experiments, we have seen that the effect of specular reflection will not be removed even if we use a very short exposure time or a very low illumination intensity. Also, from the discussion in the above section, there are only a few techniques that can deal with the saturation caused by specular reflection. For very glossy objects, the specular reflection can be attenuated with polarizers [67, 70]. But, it should be noted that sometimes the remaining diffuse light is still too weak to be used to reconstruct an accurate 3D model, even if the reconstruction is compensated with a long exposure time. Compared with the widely used sinusoidal patterns, the binary pattern is less sensitive to the effect of specular reflection [53, 61], in which the edge rather than the phase is extracted. In addition, multi-view fringe projection systems can also be utilized as long as the corresponding points from different views are not saturated at the same time [54, 69, 71].

6.1.2. Transition areas. For HDR 3D imaging, we may face surfaces with textures having distinctive reflectance changes, e.g. the checkerboard. With the reviewed techniques, we can properly handle the pixels within each homogeneous region. However, errors tend to occur at the transition areas. The reason is that due to the discrete spatial sampling, pixels at the texture boundary capture light reflected from the dark and bright areas simultaneously. The captured intensity is affected by the area of the transition region, the ratio of areas with different reflectivity, and the difference in reflectivity for the area [62]. Due to these influences, it is difficult to correctly measure the corresponding contour. Visually, these errors look like small pulses at the transition areas. As the errors show evident depth changes on retrieved 3D models, one can readily locate them and correct them with the assists of neighboring pixels. This could be effective for smooth surfaces. However, it may be fragile for geometrically complex surfaces. One promising strategy is to project binary patterns and extract the edges to recover the profile, which is less sensitive to the unreliable intensity captured at the transition areas [53, 61].

6.2. Challenges from implementation

6.2.1. Measurement efficiency. With the rapid development of digital illumination and imaging technology, many applications are beginning to require fast or in-line 3D measurements. For techniques using image fusion, if N frames of fringe images are required for a normal 3D reconstruction, one has to capture a total of mN images for an HDR 3D reconstruction where m is the number of exposure times used or the number of projections of patterns with different strength. Thus, the time cost can easily increase by m times for this kind of HDR measurement. From our discussion, the three-star methods have the highest efficiency among the reviewed techniques. Although they can recover the contour with a single measurement, some of them still have to project many patterns during the period of measurement. Intuitively, high-speed cameras and projectors can be used to reduce the time cost of image acquisition [73] but at the expense of higher investment. In contrast, the methods exploiting additional equipment or multi-view geometry have greater potential for improving the efficiency substantially, since the dynamic range can be extended without depending on the information collected temporally [54, 67–69].

6.2.2. Indirect illumination. When a scenario is lit, the radiance measured has two components: direct illumination due to direct lighting from the projector and indirect illumination caused by light reflected by other points in the scenario [89], e.g. deep holes. The indirect illumination can seriously deteriorate the HDR 3D measurements, since the reflective points can easily reflect images of their adjacent areas. Zhong *et al* [51] considered the effect of interreflection and presented a calibration method for a global optimal exposure time. Nayar *et al* [89] showed that high-frequency patterns can potentially remove the effect of indirect illumination. But, increasing the frequency also increases the signal periodicity, which makes the phase unwrapping more difficult. Inspired by this method, Chen *et al* [90] developed a promising modulated phase-shifting technique, which can remove the effect of indirect illumination for lower-frequency patterns.

6.3. Potential applications

Without applications, technology will not advance. Here, several potential applications for HDR 3D imaging with fringe projection techniques are introduced. Generally, due to their enhanced ability to deal with objects with complex surfaces, they are more flexible than conventional fringe projection techniques. Their values will be further increased by building the bridge between these techniques and other fields.

6.3.1. Quality control for surfaces. In manufacturing, quality control is a process that ensures customers receive products free from defects that meet their needs. Distortion in shapes or flaws on surfaces will adversely affect the reliability of manufactured components and reduce the product lifetime. Therefore, quality control of surfaces is important in industrial manufacturing. Due to its high precision and high efficiency, fringe projection profilometry is widely applied to inspections of surfaces. Compared with traditional fringe projection techniques, reinforced HDR 3D measuring approaches are showing higher adaptability and flexibility for scanned objects. They are good at dealing with reflective workpieces or surfaces painted with bright and dark textures, which are difficult for the traditional methods.

6.3.2. Reverse engineering. Reverse engineering, also called back engineering, is the process by which an object is deconstructed to reveal its engineering specifications and architecture. Objects with regular geometry are often generated analytically with geometric model schemes. For free-form objects which do not have regular shapes, however, it is necessary to measure them to make digital 3D records of them. Compared with contact scanning by CMM, fringe projection-based HDR 3D profilometry can obtain geometric information accurately and efficiently without physical contact. Moreover, owing to the extended dynamic range, it can inspect objects with different characteristics in terms of reflection, which reduces the difficulty in the reverse engineering of complex objects.

6.3.3. Manufacture of robots. Robots are changing the face of manufacturing nowadays. They are designed to move materials, as well as perform a variety of tasks in manufacturing and production settings. They are often used to perform duties that are dangerous, or unsuitable for human workers, such as repetitious work that causes boredom and could lead to injuries because of the inattentiveness of the worker. With HDR 3D imaging, visual ability in three dimensions will enhance the robot's capability for more applications. For example, the robot can grab objects and reconstruct the surroundings with the assists of the 3D information. Furthermore, the sensing is more robust and flexible with HDR 3D reconstructions, and is less sensitive to the appearance of scanned surfaces. The increased ability in vision will facilitate the development of more powerful robots.

6.3.4. 3D digitization of cultural heritage. Digitization is changing our cultural experience, not only in terms of new technology-based access, but also in terms of participation and creation. The digitization and online accessibility of cultural resources gives cultural heritage a clear profile on the Internet and protects cultural diversity. Digitization of cultural heritage includes the 3D digitization, management, storage, and reproduction of 3D data. As the first step, 3D digitization is very significant to the whole process of digitization. Benefitting from an enhanced dynamic range, HDR 3D measuring techniques are robust in dealing with the large variation of texture which may be caused by erosion over the years, and can deal with the reflective parts of scanned cultural relics. This merit makes them versatile for 3D digitization of cultural heritage.

6.3.5. Human body scanning. 3D body scanning can capture an entire human body, or only specific parts, to generate a detailed 3D model. As no two human bodies are alike, the scan finds its purpose basically everywhere a custom fit is called for. For example, it can be applied to shape analysis, creating personalized figurines, creating avatars, and custom fitting of equipment. Compared with conventional structured light methods, HDR 3D imaging techniques do not have requirements on the color of clothes of the scanned human, i.e. clothes with dark color are also allowed. In addition, they can measure the shiny surfaces of leather clothing, jewelry (opaque), or other accessories, which is desirable for human body scanning.

6.4. Recommendations

To better perform HDR 3D measurements with fringe projection, we recommend users to take the following measures.

- To eliminate the effect of ambient light, find a dark environment if possible. If not, increase the brightness of the projected light and decrease the size of the aperture of the camera lens.
- To use methods based on camera multi-exposure, the initial exposure time suggested is $1/F_\mathrm{p}$, where F_p is the frequency of the projector. Moreover, the increment of the following exposures should be multiples of the initial exposure time.
- For measurements of dark objects, an enhancement of the projected intensity is preferred. Although increasing the exposure time can also make the object become brighter, more ambient light tends to be captured at the same time. Moreover, the efficiency is not changed with the strong projected intensity but will be affected with prolonged exposure time. For extremely dark surfaces, one may increase the projected intensity and exposure time simultaneously.
- For measurements of shiny and smooth objects, the simplest way is to introduce polarizers which can deal with the saturation caused by either specular reflection or diffuse reflection without changing the algorithms used. If dark objects also exist, a hybrid method synthetically increasing the projected intensity or the exposure time is suggested.
- A simple yet effective way to perform HDR 3D measurements is to use the N-step phase shifting method with a large phase step, e.g. $N \geqslant 7$. It is insensitive to both saturation (caused by diffuse light) in bright areas and low SNR signal in dark regions.
- For measurements of moving shiny objects, a multi-view fringe projection system is a good choice. It can not only remove the effect of saturation but also benefit from epipolar constraint which can unwrap the phase unambiguously without increasing the number of patterns.

7. Conclusion

We have presented a comprehensive review of HDR 3D imaging techniques with fringe projection. A new classification of the reviewed techniques has been presented. In general, they can be classified into two groups: equipment-based techniques and algorithm-based techniques. The difference between the two groups is that the former calculates 3D reconstructions from processed images, e.g. images that are fused from several raw images captured with different parameters. On the contrary, the latter can extract the 3D shape information directly from raw images, e.g. images with highlights or saturated pixels. Most HDR methods belong to the first group, so this group is further subdivided into four groups: camera-based techniques, projector-based techniques, additional equipment-based techniques, and hybrid techniques. This work comprehensively reviews the methods in each group from both principles and experiments. With the experimental results and our discussion, we show the advantages and constraints of the approaches in terms of the capacity of handling surfaces with different kinds of reflection characteristic. We believe this article will be a useful guide for rapidly finding or developing a suitable HDR 3D shape acquisition technique for a given application.

Acknowledgment

This work was supported by the National Natural Science Fund of China (61705105, 61722506, 111574152), the National Key Technologies R&D Program of China (2017YFF0106403), the Final Assembly '13th Five-Year Plan' Advanced Research Project of China (30102070102), The Key Research and Development Program of Jiangsu Province, China (BE2017162), the Outstanding Youth Foundation of Jiangsu Province of China (BK20170034), the National Defense Science and Technology Foundation of China (0106173), the 'Six Talent Peaks' project of Jiangsu Province, China (2015-DZXX-009), the '333 Engineering' Research Project of Jiangsu Province, China (BRA2016407), Fundamental Research Funds for the Central Universities (30917011204, 30916011322), the Open Research Fund in 2017 of Jiangsu Key Laboratory of Spectral Imaging & Intelligent Sense (3091601410414), China Postdoctoral Science Foundation (2017M621747), and Jiangsu Planned Projects for Postdoctoral Research Funds (1701038A).

ORCID iDs

Shijie Feng https://orcid.org/0000-0001-8261-5276

References

[1] Bregler C, Hertzmann A and Biermann H 2000 Recovering non-rigid 3D shape from image streams *Proc. IEEE Conf. on Computer Vision and Pattern Recognition* vol **2** pp 690–6
[2] Dutta T 2012 Evaluation of the kinect sensor for 3D kinematic measurement in the workplace *Appl. Ergon.* **43** 645–9
[3] Su W-H 2007 Color-encoded fringe projection for 3D shape measurements *Opt. Express* **15** 13167–81
[4] Takeda M and Mutoh K 1983 Fourier transform profilometry for the automatic measurement of 3D object shapes *Appl. Opt.* **22** 3977–82
[5] Tangelder J W H and Veltkamp R C 2004 A survey of content based 3D shape retrieval methods *Proc. Shape Modeling Applications* pp 145–56
[6] Hocken R J and Pereira P H 2016 *Coordinate Measuring Machines and Systems* (Boca Raton, FL: CRC Press)
[7] Ni J and Wldele F 1995 Coordinate measuring machines *Coordinate Measuring Machines and Systems* (New York: Marcel Dekker) pp 39–74
[8] Spyridi A J and Requicha A A 1990 Accessibility analysis for the automatic inspection of mechanical parts by coordinate measuring machines *Proc. IEEE Int. Conf. on Robotics and Automation* (IEEE) pp 1284–9
[9] Besl P J 1989 *Active Optical Range Imaging Sensors* (Berlin: Springer) pp 1–63
[10] Chen F, Brown G M and Song M 2000 Overview of three-dimensional shape measurement using optical methods *Opt. Eng.* **39** 10–22
[11] Feng S, Zuo C, Tao T, Hu Y, Zhang M, Chen Q and Gu G 2018 Robust dynamic 3D measurements with motion-compensated phase-shifting profilometry *Opt. Lasers Eng.* **103** 127–38
[12] Huang D, Swanson E A, Lin C P, Schuman J S, Stinson W G, Chang W, Hee M R, Flotte T, Gregory K and Puliafito C A 1991 Optical coherence tomography *Science* **254** 1178–81
[13] Idesawa M, Yatagai T and Soma T 1977 Scanning moiré method and automatic measurement of 3D shapes *Appl. Opt.* **16** 2152–62
[14] Kemao Q 2007 Two-dimensional windowed fourier transform for fringe pattern analysis: principles, applications and implementations *Opt. Lasers Eng.* **45** 304–17
[15] Scharstein D and Szeliski R 2002 A taxonomy and evaluation of dense two-frame stereo correspondence algorithms *Int. J. Comput. Vis.* **47** 7–42
[16] Zhang Z, Towers C E and Towers D P 2006 Time efficient color fringe projection system for 3D shape and color using optimum 3-frequency selection *Opt. Express* **14** 6444–55
[17] Heist S, Lutzke P, Schmidt I, Dietrich P, Khmstedt P, Tnnermann A and Notni G 2016 High-speed three-dimensional shape measurement using GOBO projection *Opt. Lasers Eng.* **87** 90–6
[18] Tao T, Chen Q, Da J, Feng S, Hu Y and Zuo C 2016 Real-time 3D shape measurement with composite phase-shifting fringes and multi-view system *Opt. Express* **24** 20253–69
[19] Zhang Q and Su X 2005 High-speed optical measurement for the drumhead vibration *Opt. Express* **13** 3110–6
[20] Zuo C, Tao T, Feng S, Huang L, Asundi A and Chen Q 2018 Micro fourier transform profilometry (FTP): 3D shape measurement at 10 000 frames per second *Opt. Lasers Eng.* **102** 70–91
[21] Huang L, Kemao Q, Pan B and Asundi A K 2010 Comparison of Fourier transform, windowed Fourier transform, and wavelet transform methods for phase extraction from a single fringe pattern in fringe projection profilometry *Opt. Lasers Eng.* **48** 141–8
[22] Huang P S, Zhang C and Chiang F-P 2003 High-speed 3D shape measurement based on digital fringe projection *Opt. Eng.* **42** 163–9
[23] Kemao Q 2004 Windowed Fourier transform for fringe pattern analysis *Appl. Opt.* **43** 2695–702
[24] Li Z, Curless B and Seitz S M 2003 Spacetime stereo: shape recovery for dynamic scenes *Proc. IEEE Computer Society Conf. on Computer Vision and Pattern Recognition* vol 2 pp II-367–II-74
[25] Scharstein D and Szeliski R 2003 High-accuracy stereo depth maps using structured light *Proc. IEEE Computer Society Conf. on Computer Vision and Pattern Recognition* vol 1 pp I-195–I-202
[26] Su X and Zhang Q 2010 Dynamic 3D shape measurement method: a review *Opt. Lasers Eng.* **48** 191–204
[27] Zhang Z H 2012 Review of single-shot 3D shape measurement by phase calculation-based fringe projection techniques *Opt. Lasers Eng.* **50** 1097–106
[28] Zhou P, Zhu J, Su X, You Z, Jing H, Xiao C and Zhong M 2017 Experimental study of temporal-spatial binary pattern projection for 3D shape acquisition *Appl. Opt.* **56** 2995–3003
[29] Gorthi S S and Rastogi P 2010 Fringe projection techniques: whither we are? *Opt. Lasers Eng.* **48** 133–40
[30] Guo H, He H, Yu Y and Chen M 2005 Least-squares calibration method for fringe projection profilometry *Opt. Eng.* **44** 033603
[31] Hartley R and Zisserman A 2003 *Multiple View Geometry in Computer Vision* (Cambridge: Cambridge University Press)
[32] Huang L, Chua P S and Asundi A 2010 Least-squares calibration method for fringe projection profilometry considering camera lens distortion *Appl. Opt.* **49** 1539–48
[33] Reich C, Ritter R and Thesing J 2000 3D shape measurement of complex objects by combining photogrammetry and fringe projection *Opt. Eng.* **39** 224–32
[34] Schreiber W and Notni G 2000 Theory and arrangements of self-calibrating whole-body 3D-measurement systems using fringe projection technique *Opt. Eng.* **39** 159–70
[35] Feng S, Chen Q, Zuo C, Li R, Shen G and Feng F 2013 Automatic identification and removal of outliers for high-speed fringe projection profilometry *Opt. Eng.* **52** 013605
[36] Huang L and Asundi A K 2011 Phase invalidity identification framework with the temporal phase unwrapping method *Meas. Sci. Technol.* **22** 035304
[37] Lu J, Mo R, Sun H, Chang Z and Zhao X 2016 Invalid phase values removal method for absolute phase recovery *Appl. Opt.* **55** 387–94
[38] Lu J, Mo R, Sun H, Chang Z and Zhao X 2016 Simplified absolute phase retrieval of dual-frequency fringe patterns in fringe projection profilometry *Opt. Commun.* **364** 101–9
[39] Wang H, Kemao Q and Soon S H 2015 Valid point detection in fringe projection profilometry *Opt. Express* **23** 7535–49
[40] Chiang F-P, Huang P S and Zhang C 2003 High-speed 3D shape measurement based on digital fringe projection *Opt. Eng.* **42** 42–6
[41] Farid H 2001 Blind inverse gamma correction *IEEE Trans. Image Process.* **10** 1428–33
[42] Guo H, He H and Chen M 2004 Gamma correction for digital fringe projection profilometry *Appl. Opt.* **43** 2906–14
[43] Zhang S and Yau S-T 2007 Generic nonsinusoidal phase error correction for three-dimensional shape measurement using a digital video projector *Appl. Opt.* **46** 36–43
[44] Pan B, Kemao Q, Huang L and Asundi A 2009 Phase error analysis and compensation for nonsinusoidal waveforms in phase-shifting digital fringe projection profilometry *Opt. Lett.* **34** 416–8
[45] Hoang T, Pan B, Nguyen D and Wang Z 2010 Generic gamma correction for accuracy enhancement in fringe-projection profilometry *Opt. Lett.* **35** 1992–4

[46] Zhang S and Yau S-T 2009 High dynamic range scanning technique *Opt. Eng.* **48** 033604–7
[47] Qi Z, Wang Z, Huang J, Xue Q and Gao J 2016 Improving the quality of stripes in structured-light three-dimensional profile measurement *Opt. Eng.* **56** 031208
[48] Long Y, Wang S, Wu W and Liu K 2015 Accurate identification of saturated pixels for high dynamic range measurement *Opt. Eng.* **54** 043106
[49] Zhang B, Ouyang Y and Zhang S 2015 High dynamic range saturation intelligence avoidance for three-dimensional shape measurement *15th IEEE/ACM Int. Symp. on Cluster, Cloud and Grid Computing* (IEEE) pp 981–90
[50] Ekstrand L and Zhang S 2011 Autoexposure for three-dimensional shape measurement using a digital-light-processing projector *Opt. Eng.* **50** 123603
[51] Zhong K, Li Z, Zhou X, Li Y, Shi Y and Wang C 2015 Enhanced phase measurement profilometry for industrial 3D inspection automation *Int. J. Adv. Manuf. Technol.* **76** 1563–74
[52] Rao L and Da F 2018 High dynamic range 3D shape determination based on automatic exposure selection *J. Vis. Commun. Image Represent.* **50** 217–26
[53] Song Z, Jiang H, Lin H and Tang S 2017 A high dynamic range structured light means for the 3D measurement of specular surface *Opt. Lasers Eng.* **95** 8–16
[54] Feng S, Chen Q, Zuo C and Asundi A 2017 Fast three-dimensional measurements for dynamic scenes with shiny surfaces *Opt. Commun.* **382** 18–27
[55] Waddington C and Kofman J 2010 Saturation avoidance by adaptive fringe projection in phase-shifting 3D surface-shape measurement *Int. Symp. on Optomechatronic Technologies* pp 1–4
[56] Waddington C J and Kofman J D 2014 Modified sinusoidal fringe-pattern projection for variable illuminance in phase-shifting three-dimensional surface-shape metrology *Opt. Eng.* **53** 084109
[57] Zhang L, Chen Q, Zuo C and Feng S 2018 High dynamic range 3D shape measurement based on the intensity response function of a camera *Appl. Opt.* **57** 1378–86
[58] Li D and Kofman J 2014 Adaptive fringe-pattern projection for image saturation avoidance in 3D surface-shape measurement *Opt. Express* **22** 9887–901
[59] Chen C, Gao N, Wang X and Zhang Z 2018 Adaptive pixel-to-pixel projection intensity adjustment for measuring a shiny surface using orthogonal color fringe pattern projection *Meas. Sci. Technol.* **29** 055203
[60] Lin H, Gao J, Mei Q, He Y, Liu J and Wang X 2016 Adaptive digital fringe projection technique for high dynamic range three-dimensional shape measurement *Opt. Express* **24** 7703–18
[61] Lin H, Gao J, Mei Q, Zhang G, He Y and Chen X 2017 Three-dimensional shape measurement technique for shiny surfaces by adaptive pixel-wise projection intensity adjustment *Opt. Lasers Eng.* **91** 206–15
[62] Chen S, Xia R, Zhao J, Zhang H and Hu M 2017 Analysis and reduction of phase errors caused by nonuniform surface reflectivity in a phase-shifting measurement system *Opt. Eng.* **56** 033102
[63] Babaie G, Abolbashari M and Farahi F 2015 Dynamics range enhancement in digital fringe projection technique *Precis. Eng.* **39** 243–51
[64] Sheng H, Xu J and Zhang S 2017 Dynamic projection theory for fringe projection profilometry *Appl. Opt.* **56** 8452–60
[65] Qi Z, Wang Z, Huang J, Xing C and Gao J 2018 Highlight removal based on the regional-projection fringe projection method *Opt. Eng.* **57** 041404
[66] Ri S, Fujigaki M and Morimoto Y 2008 Intensity range extension method for three-dimensional shape measurement in phase-measuring profilometry using a digital micromirror device camera *Appl. Opt.* **47** 5400–7
[67] Chen T, Lensch H P A, Fuchs C and Seidel H P 2007 Polarization and phase-shifting for 3D scanning of translucent objects *IEEE Conf. on Computer Vision and Pattern Recognition* pp 1–8
[68] Salahieh B, Chen Z, Rodriguez J J and Liang R 2014 Multi-polarization fringe projection imaging for high dynamic range objects *Opt. Express* **22** 10064–71
[69] Cai Z, Liu X, Peng X, Yin Y, Li A, Wu J and Gao B Z 2016 Structured light field 3D imaging *Opt. Express* **24** 20324–34
[70] Feng S, Zhang Y, Chen Q, Zuo C, Li R and Shen G 2014 General solution for high dynamic range three-dimensional shape measurement using the fringe projection technique *Opt. Lasers Eng.* **59** 56–71
[71] Liu G-H, Liu X-Y and Feng Q-Y 2011 3D shape measurement of objects with high dynamic range of surface reflectivity *Appl. Opt.* **50** 4557–65
[72] Jiang H, Zhao H and Li X 2012 High dynamic range fringe acquisition: a novel 3D scanning technique for high-reflective surfaces *Opt. Lasers Eng.* **50** 1484–93
[73] Zhao H, Liang X, Diao X and Jiang H 2014 Rapid *in situ* 3D measurement of shiny object based on fast and high dynamic range digital fringe projector *Opt. Lasers Eng.* **54** 170–4
[74] Yin Y, Cai Z, Jiang H, Meng X, Xi J and Peng X 2017 High dynamic range imaging for fringe projection profilometry with single-shot raw data of the color camera *Opt. Lasers Eng.* **89** 138–44
[75] Jiang C, Bell T and Zhang S 2016 High dynamic range real-time 3D shape measurement *Opt. Express* **24** 7337–46
[76] Wang M, Du G, Zhou C, Zhang C, Si S, Li H, Lei Z and Li Y 2017 Enhanced high dynamic range 3D shape measurement based on generalized phase-shifting algorithm *Opt. Commun.* **385** 43–53
[77] Chen Y, He Y and Hu E 2008 Phase deviation analysis and phase retrieval for partial intensity saturation in phase-shifting projected fringe profilometry *Opt. Commun.* **281** 3087–90
[78] Hu E, He Y and Chen Y 2010 Study on a novel phase-recovering algorithm for partial intensity saturation in digital projection grating phase-shifting profilometry *Opt. Int. J. Light Electron Opt.* **121** 23–8
[79] Chen B and Zhang S 2016 High-quality 3D shape measurement using saturated fringe patterns *Opt. Lasers Eng.* **87** 83–9
[80] Bruning J H, Herriott D R, Gallagher J E, Rosenfeld D P, White A D and Brangaccio D J 1974 Digital wavefront measuring interferometer for testing optical surfaces and lenses *Appl. Opt.* **13** 2693–703
[81] Qi Z, Wang Z, Huang J, Xing C and Gao J 2018 Error of image saturation in the structured-light method *Appl. Opt.* **57** A181–8
[82] Nayar S K, Ikeuchi K and Kanade T 1991 Surface reflection: physical and geometrical perspectives *IEEE Trans. Pattern Anal. Mach. Intell.* **13** 611–34
[83] Huntley J M and Saldner H 1993 Temporal phase-unwrapping algorithm for automated interferogram analysis *Appl. Opt.* **32** 3047–52
[84] Huntley J M and Saldner H O 1997 Shape measurement by temporal phase unwrapping: comparison of unwrapping algorithms *Meas. Sci. Technol.* **8** 986
[85] Zuo C, Huang L, Zhang M, Chen Q and Asundi A 2016 Temporal phase unwrapping algorithms for fringe projection profilometry: a comparative review *Opt. Lasers Eng.* **85** 84–103
[86] Tao T, Chen Q, Feng S, Hu Y, Da J and Zuo C 2017 High-precision real-time 3D shape measurement using a

bi-frequency scheme and multi-view system *Appl. Opt.* **56** 3646–53

[87] Zhang S and Huang P S 2006 Novel method for structured light system calibration *Opt. Eng.* **45** 083601

[88] Zuo C, Chen Q, Gu G, Feng S and Feng F 2012 High-speed three-dimensional profilometry for multiple objects with complex shapes *Opt. Express* **20** 19493–510

[89] Nayar S K, Krishnan G, Grossberg M D and Raskar R 2006 Fast separation of direct and global components of a scene using high frequency illumination *ACM Trans. Graph.* **25** 935–44

[90] Chen T, Seidel H P and Lensch H P A 2008 Modulated phase-shifting for 3D scanning *IEEE Conf. on Computer Vision and Pattern Recognition* pp 1–8